Electromagnetic induction methods reveal wetland hydrogeological structure and properties

Paul McLachlan[1,1], Guillaume Blanchy[2,2], Jonathan Edward Chambers[3,3], James Sorensen[3,3], Sebastian Uhlemann[4,4], Paul Bryan Wilkinson[3,3], and Andrew Binley[2,2]

[1]Bordeaux INP
[2]Lancaster University
[3]British Geological Survey
[4]Lawrence Berkeley National Laboratory

November 30, 2022

Abstract

Understanding sensitive wetlands often requires non-invasive methods to characterize their complex geological structure and hydrogeological parameters. Here, geoelectrical characterization is explored by employing frequency-domain electromagnetic induction (EMI) at a site previously characterized by extensive intrusive measurements and 3D electrical resistivity tomography (ERT). This work investigates the performance of several approaches to obtain structural information from EMI data and sharp and smooth inversions. Additionally, the hydrological information content of EMI data is investigated using correlation with piezometric measurements, established petrophysical relationships, and synthetic modeling. EMI measurements were dominated by peat thickness and were relatively insensitive to both topography and depth to bedrock. An iso-conductivity method for peat depth estimation had a normalized mean absolute difference (NMAD) of 23.5%, and although this performed better than the sharp inversion algorithm (NMAD = 73.5%), a multi-linear regression approach achieved a more accurate prediction with only 100 measurements (NMAD = 17.8%). In terms of hydrological information content, it was not possible to unravel correlation causation at the site, however, synthetic modeling demonstrates that the EMI measurements are predominantly controlled by the electrical conductivity of the upper peat pore-water and not the thickness of the unsaturated zone or the lower peat pore-water conductivity. Additionally, a priori information significantly improves the potential for time-lapse applications in similar environments. This study provides an objective overview and insights for future EMI applications in similar environments. It also covers areas seldom investigated in EMI studies, e.g. error quantification and the depth of investigation of ERT models used for EMI calibration.

Hosted file

`supplementary information.docx` available at https://authorea.com/users/560368/articles/608420-electromagnetic-induction-methods-reveal-wetland-hydrogeological-structure-and-properties

Electromagnetic induction methods reveal wetland hydrogeological structure and properties

Authors:

Paul McLachlan[1], Guillaume Blanchy[1], Jonathan Chambers[2], James Sorensen[3], Sebastian Uhlemann[2,4], Paul Wilkinson[2], Andrew Binley[1].

Affiliations:

1 — Lancaster Environmental Centre, Lancaster University, LA1 4YQ, UK

2 — British Geological Survey, Keyworth, NG12 5GG, UK

3 — British Geological Survey, Wallingford, OX10 8ED, UK

4 — Lawrence Berkeley National Laboratory, Berkeley, CA 94720, US

ORCiD Numbers:

0000-0003-2067-3790

0000-0001-6341-5826

0000-0002-8135-776X

0000-0002-7673-7346

0000-0001-6215-6535

0000-0002-0938-9070

Data availability:

Data is currently being prepared for storage on the Pure repository via Lancaster University (http://pure.lancs.ac.uk/)

Corresponding Author:

P. McLachlan, p.mclachlan@outlook.com, pmclachlan@bordeaux-inp.fr

Current address: Bordeaux INP, EA4592 Géoressources et Environnement, Talence, France

Authorship Statement:

PM wrote the manuscript, and collected, and modeled most of the data. All co-authors provided additional comments and ideas for the manuscript. Specifically, GB contributed to the inversion methodology. JC, JS, SU, and PW provided additional data and supervised project development, additionally, JC and SU aided in preliminary data collection. AB supervised project development and experimental design.

Highlights

- Raw EMI data are highly dependent on peat thickness.
- Peat depth predictions from linear regressions were more accurate than from inverse methods.
- Reliable site-specific empirical hydrophysical models require extensive intrusive data.
- *A priori* structural data improves the ability of inverse methods to resolve dynamic processes.

Declaration of Interest:

None

Abstract

Understanding sensitive wetlands often requires non-invasive methods to characterize their complex geological structure and hydrogeological parameters. Here, geoelectrical characterization is explored by employing frequency-domain electromagnetic induction (EMI) at a site previously characterized by extensive intrusive measurements and 3D electrical resistivity tomography (ERT). This work investigates the performance of several approaches to obtain structural information from EMI data and sharp and smooth inversions. Additionally, the hydrological information content of EMI data is investigated using correlation with piezometric measurements, established petrophysical relationships, and synthetic modeling. EMI measurements were dominated by peat thickness and were relatively insensitive to both topography and depth to bedrock. An iso-conductivity method for peat depth estimation had a normalized mean absolute difference (*NMAD*) of *23.5%*, and although this performed better than the sharp inversion algorithm (*NMAD = 73.5%*), a multi-linear regression approach achieved a more accurate prediction with only 100 measurements

(*NMAD = 17.8%*). In terms of hydrological information content, it was not possible to unravel correlation causation at the site, however, synthetic modeling demonstrates that the EMI measurements are predominantly controlled by the electrical conductivity of the upper peat pore-water and not the thickness of the unsaturated zone or the lower peat pore-water conductivity. Additionally, *a priori* information significantly improves the potential for time-lapse applications in similar environments. This study provides an objective overview and insights for future EMI applications in similar environments. It also covers areas seldom investigated in EMI studies, e.g. error quantification and the depth of investigation of ERT models used for EMI calibration.

1 Introduction

The shallow subsurface structure of wetlands governs their ability to provide important hydrological and biogeochemical functions. For instance, the geometry of deposits and underlying bedrock, and their associated hydrogeological properties dictate the exchange of water, nutrients, and pollutants between surface waters and groundwaters. Before the 1970s the importance of wetlands was commonly overlooked, and they were often modified; e.g. for agriculture or commercial and residential development (see Davidson, 2014). Since then there has been significant effort in restoring, maintaining, and managing wetlands (see Wagner et al., 2008). These efforts require methods for wetland characterization. However, conventional methods such as lithological sampling or piezometer installation (e.g. Grapes et al., 2005; Allen et al., 2010) may have limited spatial coverage or be prohibited due to environmental damage they may cause.

Alternatively, hydrogeophysics provides the potential for subsurface characterization at high spatial and temporal resolutions (see reviews by Binley et al., 2015; Singha et al., 2015; Parsekian et al., 2015; McLachlan et al., 2017). Methods sensitive to electrical conductivity are of interest to wetland characterization as it is dictated by porosity, pore-water conductivity, saturation, and grain mineralogy. These methods can therefore be used to distinguish between different lithologies and elucidate hydrogeological behavior. Most hydrogeophysical wetland investigations use electrical resistivity tomography (ERT) due to their proven application in imaging lithology and monitoring hydrological states (e.g. Chambers et al., 2014; Miller et al., 2014; Walter et al., 2015; Uhlemann et al., 2016). Recently, frequency-domain electromagnetic induction (EMI) methods have increased in popularity, particularly given the ease at which relatively large areas can be surveyed (e.g. von Hebel et al., 2014; Rejiba et al., 2018; Beucher et al., 2020). Additionally, it is important to note several wetland applications of ground penetrating radar which have revealed stratigraphy (e.g. Comas et al., 2005), gas content (e.g. Slater et al., 2007), and peat pipes (e.g. Holden et al., 2003).

Initially, EMI methods were predominantly used for mapping (e.g.Sherlock and McDonnell, 2003; Corwin, 2008). However, the developments of multi-coil and multi-frequency devices, and inversion algorithms (e.g. Monteiro-Santos, 2004; Auken et al., 2015; McLachlan et al., 2020a), are such that applications have shifted focus to obtain quantitative models of electrical conductivity. In this way, EMI characterization of wetlands can be two-fold: i.e. boundaries between contrasting electrical conductivity can be interpreted in terms of stratigraphy, and electrical conductivity can be converted to parameters of interest using petrophysical models.

Recently, there have been several studies using EMI inversion to investigate wetlands, peatlands, and fluvial environments. For instance, von Hebel et al. (2014) presented an inversion algorithm for sharp inversion (where conductivities and layer thicknesses were both solved as parameters) and Frederiksen et al. (2017) employed a smooth inversion algorithm and an iso-resistivity method for extracting lithological boundaries. Additionally, Beucher et al. (2020) used both sharp and smooth inversions but concluded that predictions from linear regressions with raw data were best for structural characterization when comparing with a limited intrusive data set. Moreover, Brosten et al. (2010) investigated the link between EMI and hydraulic conductivity with a smooth inversion algorithm. The distinction between sharp and smooth inversions is important; e.g. although conductivity will vary smoothly in broadly homogenous units with varying water content or gradual changes in mineralogy, for distinctly stratified environments, regularisation will smooth any abrupt changes in electrical conductivity. However, these previous studies, while focusing on particular applications, have not provided an objective comparison of those different approaches on a well-characterized site.

The overriding aim of this work is to assess the best modeling approaches to obtain realistic estimates about properties, or states, relevant to wetland function using EMI methods. The work focuses on a previously well-characterized site, which comprises peat and gravel deposits overlying Chalk bedrock. Firstly, the best approach for assessing the peat thickness is determined; predictions from linear regressions and smooth and sharp inversion methods are validated against an extensive intrusive data set. Secondly, the ability of EMI to characterize hydrogeological properties (i.e. unsaturated zone thickness, pore-water conductivity, hydraulic conductivity, and porosity) are investigated. Lastly, the potential of EMI to resolve hydrological states is quantified using synthetic modeling to better understand the limitations of the EMI method. Furthermore, although time-lapse EMI approaches have successfully resolved soil water dynamics in agricultural sites (e.g. Whalley et al., 2017) their potential in wetland sites has not yet been explored. Therefore, this work provides a thorough investigation of the usage of EMI methods in wetland environments and provides insights for future work in similar environments.

2 Methods

2.1 Field Site

The Boxford Wetland, Berkshire, UK, covers an area of 10 ha and is situated along the River Lambourn. The river, and its associated habitats, are among the least impacted of the Chalk river systems in the UK; furthermore, the Boxford Wetland is a designated Site of Special Scientific Interest (Natural England) and a Special Area of Conservation (EU Habitats Directive) owing to the habitat it provides for aquatic and terrestrial fauna and flora (Old et al., 2014). The wetland consists of a north and a south meadow that are dissected by the Westbrook Channel (Fig. 1).

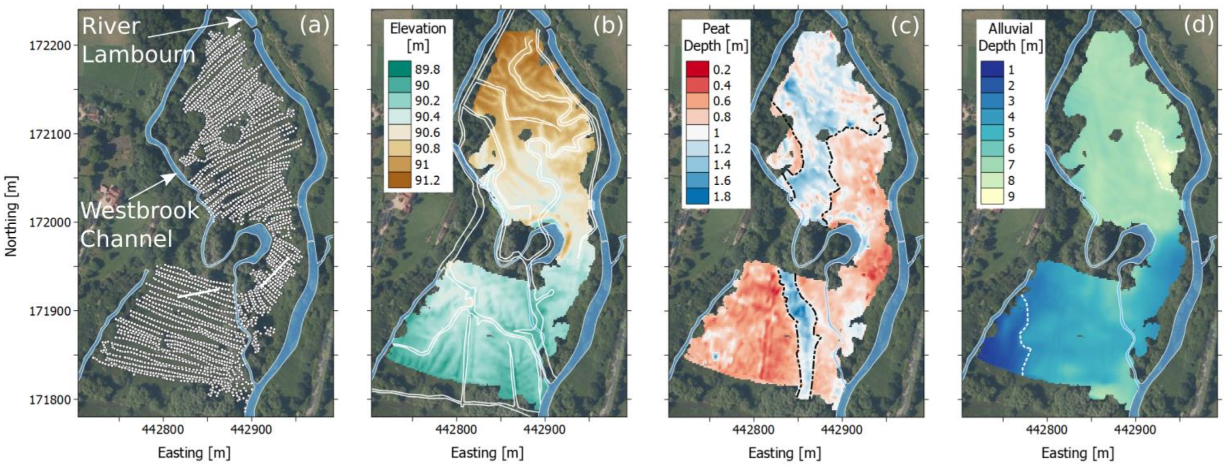

Figure 1 — Maps of (a) measurement location of peat depths (grey dots) and ERT transects used for EMI calibration (white lines), (b) topography and 18th-century channels, (c) peat depth and peat channel outline, and (d) alluvial (peat and gravel) depth from previous 3D ERT work (Chambers et al., 2014; Newell et al., 2015).

Although minimally impacted, during the 18th century the hydrology of the site was modified by a network of drainage ditches, which are still evident in the topography of the site (Fig. 1b). Furthermore, some of these channels were demonstrated to coincide with the locations of groundwater-dependent flora and sites of upwelling of groundwater (see Fig. 3, House et al., 2015).

The underlying Chalk bedrock present at the site is thought to exert a control on the hydrology. This is primarily because the upper surface of the Chalk is characterized by a discontinuous, low permeability, 'putty chalk' layer created by chemical weathering. Areas where the 'putty chalk' is absent or the Chalk has been deeply eroded, e.g. the channel feature in the north meadow (see Fig. 1d), are thought to be areas of preferential groundwater upwelling (Younger et al., 1988; Chambers et al., 2014; House et al., 2016).

Overlying the Chalk surface are Late Pleistocene to Holocene alluvial gravels and finer-grained deposits comprising peats, and alluvial silts and clays. The geometry of these deposits was revealed by the 3D ERT survey of Chambers et al. (2014) who observed that the gravels were thicker and more continuous in the north meadow (see Fig. 1d) and that the peats formed a broadly north-south trending channel on top of the gravels (see Fig 1c). A more detailed lithological study by Newell et al. (2015) demonstrated that the gravels can be divided into a unit of chalky gravels and an overlying unit of coarser flinty gravels, with some upper gravels showing the development of lateral accretion surfaces. The overlying deposits comprise a mixture of peats and alluvial clays and silts (see Newell et al., 2016); for the sake of brevity, these mixed peat deposits are referred to as peats hereafter. Organic carbon analysis of these peat deposits by Newell et al. (2016) indicated that they were deposited over 4,000 years ago and contain organic matter from both aquatic and terrestrial sources; i.e. the site was characterized by periodic changes in climate wetness. The complex depositional history of the peats is further evidenced by time-lapse ERT studies (Uhlemann et al. 2016; McLachlan et al., 2020b) who demonstrated that the peats contain several hydrologically distinctive units. Most notably, the peats comprise an upper and lower layer separated by a thin clay layer. Both layers typically remain hydrologically separate and only exchange water when large hydraulic gradients are present, e.g. due to abrupt changes in the river stage and groundwater, which are strongly linked (Old et al., 2014).

2.2 Intrusive Data

The measured peat depths (see Fig. 1a) used to validate the peat thickness predictions from the EMI data here are taken from Chambers et al. (2014). Measurements were made by pushing a 6 mm diameter steel rod into the subsurface. The gravel was assumed non-penetrable and the depth was determined from the maximum penetration depth of the rod. Measurements were made at 2815 locations on an approximate grid with 5 by 5 m spacing. In six locations the peat depths were too deep and were assumed to be 1.86 m, i.e. the maximum depth achievable with this method.

During the EMI data collection (05-Mar-18 to 08-Mar-18), hydrological measurements were obtained from the peat and gravel piezometers at the site. In total 12 measurements of the unsaturated zone thickness in the peats and 13 measurements of pore-water electrical conductivity were obtained from both the peat and gravels. Piezometers were purged twice to ensure that pore-water conductivity measurements were representative. As the screens of many of the piezometers had become overgrown since their initial installation, a previous set of unpublished hydraulic conductivity measurements, obtained using the falling head method, were used for analysis. This included 19 hydraulic conductivity measurements for the gravels and 20 for the peats.

Additionally, as also noted by Beucher et al. (2020), there is interest in characterizing the organic matter content of wetland sediments given their role in the global carbon cycles (see Mitsch and Gosselink, 2007). To address this, 24 auger cores were obtained across the site and subsampled into 0.1 m sections; organic matter content was then determined using the loss on ignition method (Heiri et al., 1999). Although a positive correlation between electrical conductivity and organic matter content may be expected given the surface conductivity component of organic sediments observed by Comas and Slater (2004), here no significant relationships were found between raw or inverted EMI data and organic matter content. This is perhaps due to the high organic matter content of peats at the site and the limited variability between samples, i.e. organic carbon content is not the main driver of variability in bulk electrical conductivity. Consequently, these data are not discussed further; however, this is a potential avenue for future research.

2.3 Geophysical Data Collection

2.3.1 EMI Data Collection

EMI methods measure the interaction between an induced primary electromagnetic field and the resultant secondary electromagnetic field. Here, EMI data were obtained using the GF Instruments CMD Explorer device (Brno, Czech Republic), hereafter referred to as the GF Explorer. This device contains three receiver coils with transmitter-receiver separation distances of 1.48, 2.82, and 4.49 m. Furthermore, it can be operated with coplanar coils orientated either vertically (VCP) or horizontally (HCP), with respect to the ground, meaning that in total 6 measurements can be obtained. Hereafter, the GF Explorer measurements are referred to as VCP1.48, VCP2.82, VCP4.49, HCP1.48, HCP2.82, and HCP4.49, to indicate the coil orientation and spacing.

In most cases, EMI devices like the GF Explorer are operated on, or near, the ground surface, however, at the Boxford Wetland, the presence of dense vegetation required that the device be manually carried at 1 m above ground level. This has implications for the depth sensitivity of the instrument. For instance, the depth of investigation values (i.e. the depth above which 70% of the signal comes from (see Callegary et al., 2007)) for the specifications of the GF Explorer are 1.1, 2.2, and 3.4 m in VCP mode, or 2.1, 4.2, and 6.7 m in HCP mode when the device is operated at ground level. However, when operated at 1 m elevation the sensitivity patterns are shifted; following Andrade and Fischer (2018), the recalculated depth of investigation values become 2.7, 3.4, and 4.5 m for VCP mode, and 3.1, 4.6, and 6.9 m for HCP. Although the sensitivity patterns for VCP and HCP measurements are both shifted deeper, the effect is greater for VCP measurements. Essentially this means that when operated at 1 m elevation the sensitivity patterns of the EMI measurements become more similar (i.e. less independent) and there is less sensitivity to the shallowest subsurface.

Before the field measurements, the GF Explorer was left for 30 minutes to allow it to stabilize. For each survey, the device was carried at 1 m and held perpendicularly to walking direction. Although in some places the ground was heavily vegetated, uneven, and/or boggy, care was taken to ensure that the GF Explorer remained in a stable position during surveying. For instance, changes in the elevation of the device, its orientation to the ground, and its rotation about its long axis will all have implications on the quality of measurements. Nonetheless, to assess measurement quality, perpendicular survey lines were collected; this also enabled the assertation of whether any processing steps, e.g. drift corrections (as determined from a central drift station) or ERT calibration (see section 2.3.2) introduced any biases into the data. Measurements were logged every second and paired with coordinates obtained from a Trimble GPS (Sunnyvale, California, US) which has an accuracy of < 3 m; additionally, logged coordinates were shifted using 8 control points that were previously surveyed using a differential GPS.

2.3.2 ERT Data Collection

Although EMI devices provide an independent measure of electrical conductivity, several authors have advocated for calibrating EMI measurements before inversion (e.g. Lavoué et al., 2010; Minsley et al., 2013; von Hebel et al. 2014). Here, ERT data are used to calibrate EMI data following the same general approach of Lavoué et al. (2010); unlike EMI, ERT is not subject to drift or calibration issues. ERT methods use measurements of transfer resistance to construct models of electrical resistivity. ERT measurements are collected using two pairs of electrodes; one pair to inject current and the other pair to measure the resultant electrical potential difference. By utilizing different combinations of electrodes with different spacings, different regions of the subsurface can be interrogated. It is important to note that the calibration of EMI data using ERT data implicitly assumes that the ERT model is correct, and any biases will be inherited into the EMI data. Also, both methods have different spatial resolutions, and ERT is sensitive to resistors whereas EMI is sensitive to conductors which may also impart biases into the EMI data. Nonetheless, ERT calibration has been shown to aid with the convergence of inverse EMI models (e.g. von Hebel et al., 2014; 2019).

Two ERT data sets were collected, one in each meadow, (Fig. 1a). The locations of the ERT transects were selected to encompass ground with variable peat depths. Both transects were 47.5 m long and comprised 96 electrodes at 0.5 m spacing. Measurements were made using a dipole-dipole sequence and a Syscal Pro resistivity device (IRIS Instruments, Orleans, France). Before and following the collection of ERT data, plastic pegs, and string were used to mark the position of both transects to obtain EMI measurements in the same position as ERT measurements during respective surveys. Both data sets were inverted on a quadrilateral finite element mesh using R2 via the ResIPy software (see Blanchy et al., 2020), and the depth of investigation was determined using the method proposed by Oldenburg and Li (1999). Both data sets were inverted for a quadrilateral mesh allowing for a 2% measurement error to compensate for forward modeling errors associated with the mesh. In both cases, convergence was achieved in 3 iterations.

2.4 EMI Data Filtering and Calibration

EMI devices typically provide data in terms of an apparent electrical conductivity (*ECa*) via the low induction number approximation (see McNeill, 1980). The *ECa* values obtained by the GF Explorer are derived using an alternative manufacturer calibration, therefore before inversion *ECa* values were converted such that they are coincident with the EMI forward model used in the inverse algorithm, which uses the low induction number approximation (see McLachlan et al. 2020a). Furthermore, it is important to note that although non-linear methods exist for obtaining more representative *ECa* values from quadrature conductivities (e.g. Andrade et al., 2016), these approaches will have minimal influences on inversion results, especially in low conductivity environments.

As the GF Explorer does not provide a measure of data quality in continuous logging mode, measurements that differed by more than 5% from both preceding and succeeding measurements were considered poor quality and replaced via linear interpolation to smooth the data. Following this, data were binned based on their *ECa* values into 16 equally spaced bins. Any data in bins that contained less than 0.5% of the total data were considered outliers; these were also removed and replaced via linear interpolation. Data from each survey were then corrected based on measurements made at the drift station, this was done separately for each EMI data set.

The EMI measurements used for calibration were obtained during each survey; measurement coordinates were converted into a distance along the relevant ERT transect. The forward model response of each column of the quadrilateral ERT model was computed using the Maxwell-based forward models for each of the six measurement specifications of the GF Explorer and then converted to *ECa* values using the low induction number approximation. To account for the different spatial resolutions of ERT and EMI methods, a running average across 3 samples (~1 m) was applied, and data were then binned based on their position along the ERT transect, for which bin widths of 1 m were used. Additionally, the ERT depth of investigation, as computed by the Oldenburg and Li (1999) method, provided a metric by which to objectively avoid using EMI measurements obtained at locations along the ERT transect with poor depth sensitivity. Here, locations along the ERT transect where the depths of investigation were less than 1 m were not included. The coefficients from linear regressions for each measurement setup were then used to calibrate the remainder of the EMI data.

2.5 EMI Error Quantification

As noted, perpendicular survey lines were collected to quantify errors within the data and determine if data processing had been effective. The errors were quantified by first locating cross-over points (i.e. locations of approximately perpendicular survey lines) within the VCP and HCP data sets. The mean and standard deviations were then computed for all measurements made within a two-meter radius of these cross-over points. By plotting these errors through time, it was evident that drift had been accounted for and no substantial errors were introduced by any of the processing steps (e.g. by drift correction or ERT calibration). The overall errors of the EMI data were low and showed a dependence on the magnitude (Fig 2). For instance, expressed as a percentage the errors for VCP1.48, VCP2.82, VCP4.49, HCP1.48, HCP2.82, and HCP4.49 were 6.26, 3.72, 3.64, 3.30, 1.46, and 1.88%, respectively. This suggests that throughout the surveying the position of the device relative to the ground may have been unstable. For instance, it could be anticipated that errors arising from orientation or elevation issues would be higher in higher conductivity regions of the wetland as the ratio of air to subsurface conductivity would be increased. Although this could explain why the measurements with a lower depth of investigation have higher errors, it is important to note that such an effect could also arise from the variable vegetation cover at the site.

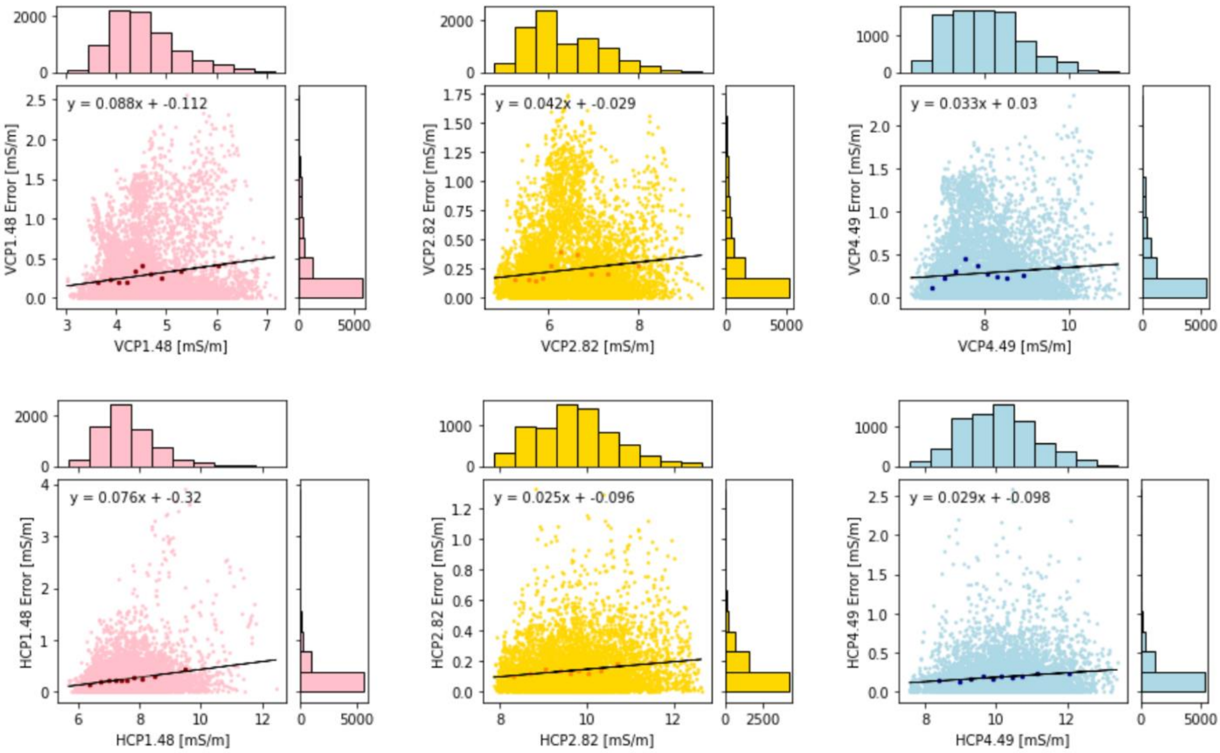

Figure 2 — Errors of EMI measurements show the relationship between *ECa* and error for VCP1.48, VCP2.82, VCP4.49, HCP1.48, HCP2.82, and HCP4.49 respectively.

2.6 EMI Inversion

Before inversion, EMI measurements were co-located by interpolating data onto the coordinates of the intrusive peat depth measurements using inverse distance weighting. Only peat depth measurement locations that had > 3 EMI measurements made within a 5 m radius were considered, this resulted in a co-located data set comprising 2308 measurements, out of the total 2815 peat depth measurements collected. These data were inverted using the Maxwell-based forward models implemented in EMagPy (McLachlan et al., 2020a). As with other EMI inversion software the smooth inversion uses vertical regularisation to balance the overall data misfit and model smoothness. This avoids geologically unreasonable models at the expense of smoothing the electrical conductivity. In comparison, for the sharp inversion algorithm used here, regularization is not implemented, and depths of interfaces are treated as parameters.

The smooth inversions were completed for an 11-layer model (depths = 0.2, 0.4, 0.6, 0.8, 1.0, 1.2, 1.4, 1.8, 2.4, 3 m) and a vertical smoothing factor of 0.01. This approach assumes that beyond 3 m the subsurface is homogenous. However, in many cases, the boundary between the gravels and Chalk was deeper (Fig. 1d). These depths were chosen because in most cases the conductivity profile was monotonic (see supplementary information), i.e. there was unsubstantial sensitivity to resolve the Chalk.

For the sharp inversions, a grid-based parameter search method (e.g. Dafflon et al., 2013) was used to produce two-layer models. This approach also assumes that the Chalk and gravel were indistinguishable. This assumption is justified by the insignificant reduction in misfit when comparing 2 and 3-layer models (see supplementary information). Parameter values of 1 to 50 mS/m in 1 mS/m increments and 50 to 150 mS/m in 2 mS/m increments were chosen for the electrical conductivity values of layers 1 and 2, and the parameters for the thicknesses of layer 1 were 0.1 to 3 m in 0.1 m increments. The best model for each set of EMI measurements was determined from the lowest total misfit. Following this, to determine the effect of constraining the depth of layer 1 to the measured peat thickness, the model with the lowest misfit was then selected from the models with the correct peat depth (rounded to nearest 0.1 m).

2.7 Structural Characterization

The correlation between the calibrated *ECa* measurements of each coil and the elevation, measured peat depths, and alluvial thickness (e.g. combined peat and gravel thickness) were assessed using linear regressions. Following this, peat depths were estimated using a method where multi-linear regression models between the six EMI measurements and the peat depths were built. Moreover, although the most robust linear regression would be determined from all the intrusive measurements, the interest here was in determining the minimum number of intrusive measurements needed to develop a model that characterizes peat depths accurately, i.e. the point beyond which addition of intrusive data does not improve results. To do so multi-linear regressions were fitted with 20, 25, 30, 35, 45, 55, 65, 75, 85, 100, 150, 200, 250, 400 and 480 randomly sampled sets of the co-located data. The resultant coefficients were then used to predict peat depth for the remainder of the data set. To assess the ability of the linear regression to predict peat depth the normalized mean absolute difference (*NMAD*) was determined by:

$$NMAD = \frac{\sum_{i=1}^{n}\left(\frac{|d_{meas,i} - d_{pred,i}|}{d_{meas,i}}\right)}{n} \tag{1}$$

where, d_{meas} and d_{pred} are measured and predicted depths, respectively, and n is the number of observations. Furthermore, to ensure that predictions of the accuracy were robust, the multi-linear regressions were constructed 5000 times for each subset using randomly sampled data.

Peat depths were also estimated from the inverted EMI models. For the smooth models, the peat-gravel boundary was extracted using two classes of edge detection method: gradient methods and iso-surface methods. For the gradient methods, the subsurface conductivity and resistivity gradient were calculated, and the peat-gravel interface was assumed to be the depth with the steepest gradient. For the iso-surface method, single values of conductivity and resistivity were used to predict the depth of the peat-gravel interface across the whole site. As with the linear regression method, the performance of gradient and iso-surface methods was assessed by calculating NMAD. For the sharp method, the predicted peat depth was simply taken as the thickness of the upper layer of the two-layer model for the cases where *a priori* knowledge of peat depths was not supplied.

2.8 Hydrogeological Characterization

For the hydrogeological parameters, it was anticipated that there would be a negative correlation between EMI data and the unsaturated zone thickness, and a positive correlation with the pore-water conductivity. For hydraulic conductivity, the expected correlation could be positive or negative. For instance, if the electrical conductivity is dictated by porosity, a positive correlation would be expected, whereas if the electrical conductivity is dictated by clay content a negative correlation would be anticipated (e.g. see Brosten et al., 2011).

As with the structural data, linear regressions between the calibrated *ECa* measurements of each coil and the hydrogeological data were first investigated. Following this, the correlations between the modeled electrical conductivities and the hydrogeological data were investigated. For the smooth models, conductivity values were determined for the peats and gravels by using the measured peat depths to determine which model layers were in the peats and which were in the gravels. Although Brosten et al. (2011) selected a single layer for correlation with hydraulic conductivity such an approach requires, or at least assumes, that there is no thickness variation in the lithological units across the site. For the unconstrained sharp inversions, correlations between the hydrogeological properties of the peat and layer 1 were investigated, whereas the hydrological properties of the gravel were correlated with layer 2.

Additionally, the modeled electrical conductivities were used to predict the porosity. Given that the gravels are fully saturated, and the surface conductivity is negligible, the porosity can be determined from Archie's (1942) law, as follows:

$$\sigma_b = \Phi^m \sigma_w, \quad (2)$$

where σ_b is the bulk conductivity of the gravels, Φ is the effective porosity, m is the cementation factor, here assumed to be 1.5, and σ_w is the pore-water conductivity. To account for surface conductivity associated with organic matter, Comas and Slater (2004) proposed a modified Archie's (1942) law:

$$\sigma_b = \Phi^m S^n \sigma_w + \sigma_{surf}, \quad (3)$$

where S represents saturation, n is the saturation exponent and σ_{surf} is the surface conductivity and is dependent on the pore-water conductivity. Here, σ_{surf} was estimated by the pore-water conductivity using the experimental findings of Comas and Slater (2004). Although in each piezometer measurement the water table was not at the surface (i.e. the peat was not fully saturated), preliminary inversions with the constraint of a sharp three-layer model with knowledge of the unsaturated zone thickness and peat depth resulted in models with high electrical conductivity estimates of the unsaturated zone. This was in contrast with the anticipated lower saturation and could be attributed to a lack of sensitivity in this region or the presence of vegetation in regions modeled as infinitely resistive. Although such occurrence could be avoided using regularisation or further constraint, for porosity prediction, the peats were assumed fully saturated.

It is also important to draw attention to the petrophysical work of Walter et al. (2015), who found a strong relationship between bulk electrical conductivity and pore-water conductivity. Although such a relationship provides alternative routes to obtain estimates of formation factors, ultimately such an approach was not applicable here as such a relationship between bulk conductivity and pore-water electrical conductivity was not observed. This is probably due to the low variability in porosity observed by Walter et al. (2015).

Additionally, to further explore the ability of EMI to resolve hydrological processes synthetic modeling was used. Although preliminary EMI data were obtained to investigate this, there were no spatially coherent patterns of changes in EMI data and no ERT data from contemporaneous dates were available to calibrate data before EMI inversion. For synthetic modeling, the subsurface was represented by a four-layer model, i.e. the unsaturated peats, the upper and lower peats identified by Uhlemann et al. (2016), and the underlying gravel.

Pore-water logging by Uhlemann et al. (2016) showed that the peat pore-water electrical conductivities exhibited a cyclical nature reaching a maximum of ~70 mS/m in the fall (autumn) and a minimum of ~55 mS/m in the spring. In comparison, the gravel pore-water conductivities remain relatively stable and range from ~55 mS/m to ~60 mS/m throughout the seasons (see Fig. 5 of Uhlemann et al., 2016). EMI data were simulated for the specifications of the GF Explorer operated at 1 m for synthetic models representing changes in pore-water conductivity and thickness of the unsaturated peat. The bulk conductivities were determined using equation 3 for layers 1 to 3 and equation 2 for layer 4 for 20 different 'hydrological state-changes' (e.g. changing pore-water electrical conductivity) at 50 ‘locations’ (e.g. constant porosities and layer thicknesses) see supplementary information for more details.

3 Results

3.1 ERT Data and *ECa* Patterns

The ERT sections show a clear two-layer stratigraphy comprising a conductive upper layer and a more resistive lower layer (Fig. 3). Also, the measured peat depths are coincident with this boundary. Consequently, the peat has an average conductivity of 20–30 mS/m whereas the gravel has an average conductivity of 5-10 mS/m. This agrees with Chambers et al. (2014) who observed that the peat had a conductivity of 30 mS/m in the north meadow and 20 mS/m in the south meadow, whereas the gravel had a conductivity of around 4–5 mS/m in both meadows. These values are in good agreement and the small deviation can be explained by the different season and year that the data were collected. Although Chambers et al. (2014) were able to resolve the underlying Chalk with a conductivity of 6–8 mS/m, the Oldenburg and Li (1999) depth of investigation values here are relatively shallow and such a distinction was not possible. The superior depth sensitivity of Chambers et al. (2014) can be attributed to their larger electrode separation and larger survey scale.

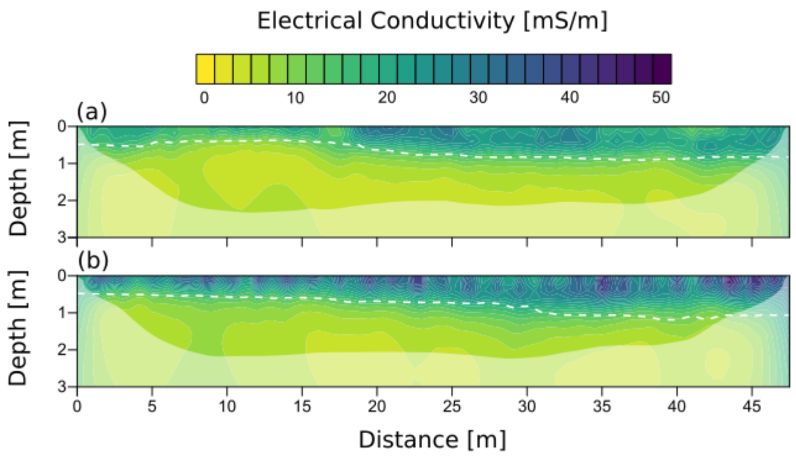

Figure 3 — ERT models of (a) north and (b) south meadow (see Fig. 1a for locations). Values are expressed in electrical conductivity; the white dashed line denotes the depth of the intrusively derived peat-gravel boundary.

The general patterns of EMI measured *ECa* coincide well with the peat depths, e.g. the geometry of the north-south trending peat channel is expressed as a conductive anomaly in the *ECa* data (Fig. 4). Additionally, in the SW corner of the south meadow, the zone of elevated *ECa* is coincident with areas where the gravels are thin, i.e. the Chalk bedrock is closer to the surface (Fig. 1d). It can also be seen in the north meadow that the zone of lower *ECa* values could correspond with the paleo-depression in the Chalk surface identified from ERT results (Chambers et al., 2014; Newell, et al., 2015), although it is important to note here that the feature also corresponds to areas where the peat depths are shallowest. Lastly, although there were slight differences in the patterns of the *ECa* data for the different coil specifications they were all greater where the peat depth is thickest and smaller where the peat depths are thinnest.

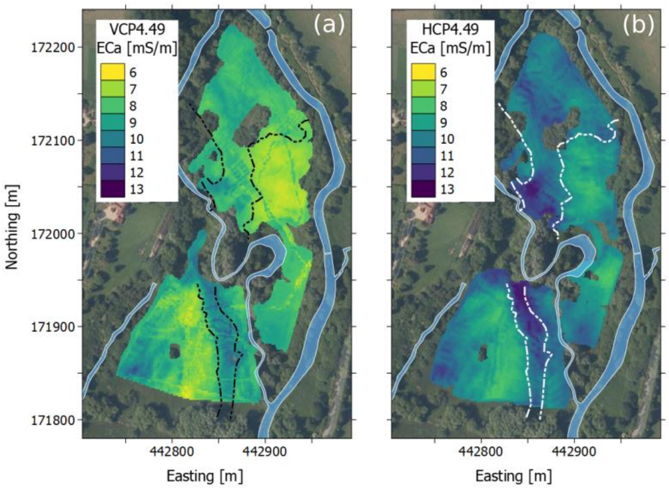

Figure 4 — Maps of *ECa* measurements from (a) VCP4.49 and (b) HCP2.82, depths of investigation are 4.5 and 4.6 m, respectively. Dashed lines indicate the position of the peat channel.

3.2 Structural Characterization

The information of each GF Explorer measurement was quantified by fitting linear regressions between the calibrated *ECa* values and the available structural information, see Fig. 5. As expected from Fig. 4, it is evident that *ECa* measurements are primarily influenced by the peat thickness; the strongest correlations are for VCP4.49 and HCP2.82 (depth of investigation values are 3.5 and 3.6 m, respectively). Furthermore, although the other parameters show significant relationships, the correlation coefficient, *r*, values are typically low to moderate. For instance, it could have been that EMI data were correlated with the peat disturbance during the 18th century (e.g. Fig. 1b), however, EMI measurements were unable to resolve this. Moreover, although in some areas the gravel thicknesses agree with the EMI data (e.g. SE corner of the south meadow), this correlation is not present across the entire site and is likely only important when peats are relatively thin.

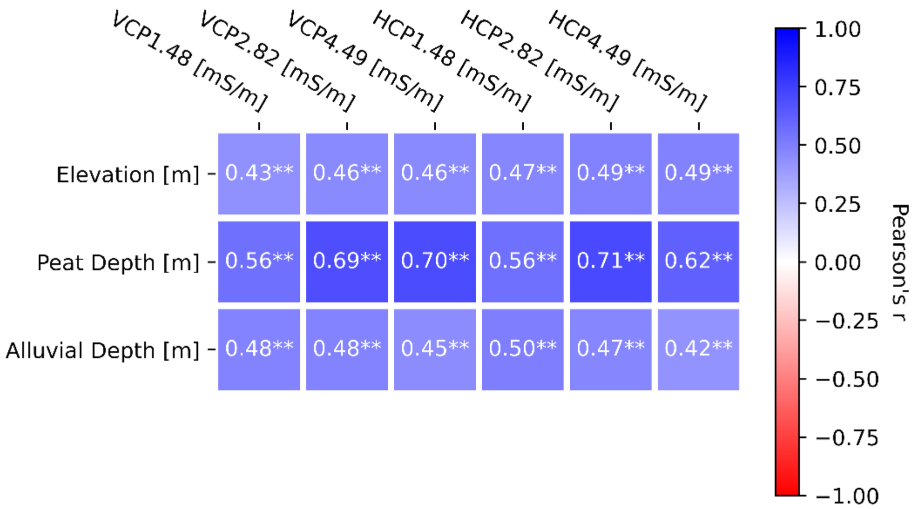

Figure 5 – Correlation plots of calibrated *ECa* measurements and structural information, in all cases n = 2308. Alluvial depth corresponds to the thickness of both peats and gravels, i.e. the depth to the Chalk bedrock. Significance levels are indicated as follows: * represents $p < 0.05$ and ** represents $p < 0.01$.

It is shown in Fig. 6b that for multi-linear regressions using > 200 observations, the data-model misfit, in terms of NMAD, is not reduced substantially. For instance, in comparing the predictions from 200 and 400 observations, the average NMAD is only reduced from 17.8% to 17.4%. Furthermore, the predicted peat depth from 100 intrusive measurements (see Fig. 6a) resolves the overall patterns of the peat depth and with reasonable accuracy (NMAD = 18.3%). However, it can be seen from Fig. 6c that areas, where the peats are thickest, are underestimated, and areas, where the peats are thinnest, are overestimated. Furthermore, although the peat depths can explain most of the variation in the EMI data ($r = 0.73$), it is anticipated that additional variability may be attributed to hydrogeological heterogeneity within the peats and/or gravels.

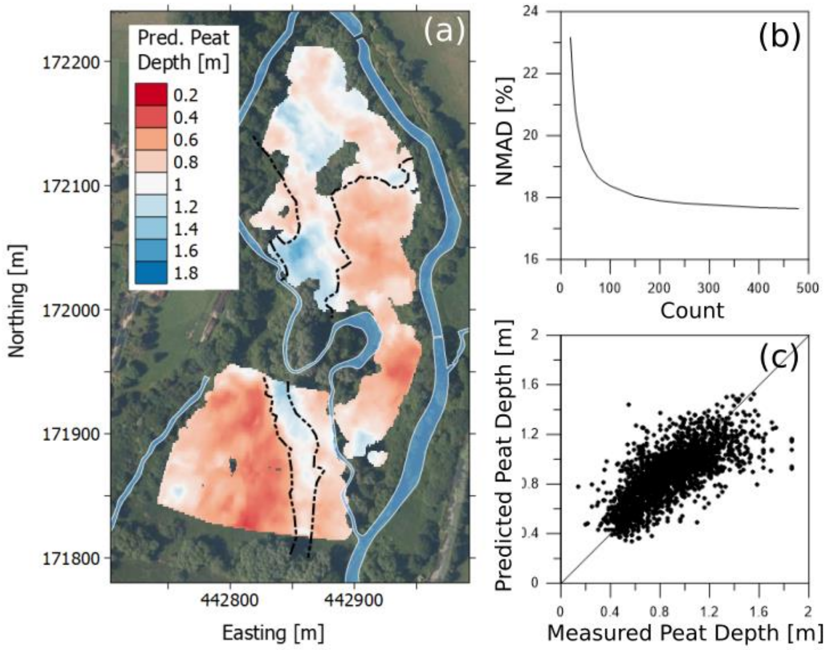

Figure 6 — Predicted peat depths based on the linear regression: (a) shows the distribution of peat depths, (b) shows the improvement in terms of normalized mean absolute difference when more observations are included, (c) shows a scatter plot of predicted and measured peat depths with 1:1 line. Dashed lines in (a) indicate the position of the peat channel. Note color scale in (a) is the same as in Fig. 1b.

Layer 3 (0.6 m depth) and Layer 9 (2.4 m depth) of the smooth inversion are shown in Fig. 7a and b. As expected, the electrical conductivity decreases with depth and the area corresponding to the peat channel occurs as a zone of elevated electrical conductivity. Of the edge detection methods investigated, the iso-conductivity method performed the best (i.e. NMAD values for iso-conductivity, iso-resistivity, resistivity gradient, and conductivity gradient methods were 24.5, 27.7, 32.5, and 37.3%, respectively). The predicted peat depth, obtained by assuming the peat-gravel boundary can be represented by an iso-surface with a conductivity of 16.5 mS/m is shown in Fig. 7c; the corresponding 1:1 plot is shown in Fig. 7d. Although the general pattern of the peat channel is well resolved, the predicted peat depths were less accurate than the predictions from the multi-linear regression method. Moreover, the predictor performs poorer for thicker peats, this could be attributed to the lower sensitivity (i.e. reduced model resolution) at these depths.

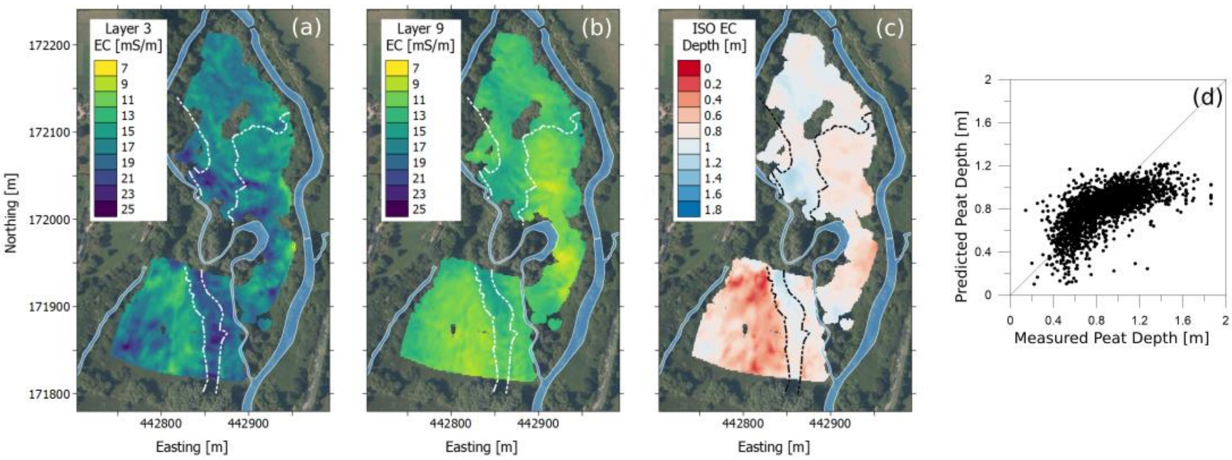

Figure 7 — Inverted electrical conductivity for smooth inversion: (a) and (b) show the inverted electrical conductivities of layers 3 (0.4 to 0.6 m) and 9 (1.8 to 2.4 m), respectively, (c) and (d) show the distribution of predicted peat depths and a scatter plot of predicted and measured peat depths, respectively. Note color scale in (c) is the same as in Fig. 1b and 6a.

The results for the sharp model approach are shown in Fig 8a, b, and c. The general pattern of the peat depth (Fig. 8c) is evident, however in most cases, the predicted peat depths are overestimated (Fig. 8g), and the predictions have an NMAD of 73.5%. Furthermore, the conductivities of layer 1 (Fig. 8a) are correlated with the modeled peat depth (r = -0.60, $p < 0.01$); i.e. high conductivity regions occur where the depth of layer 1 is shallowest, and vice versa. This correlation is also evident in the electrical conductivities of layer 2 (Fig. 8b). Such features imply that patterns in the data resulting from the peat depth are not accounted for properly in the inversion. This is further evidenced in the modeled electrical conductivities of layers 1 and 2 for the cases where *a priori* knowledge about the peat depth is supplied (Fig 8e and f) as such correlations are not present in the inversion results. Moreover, it can be seen from the histograms of modeled electrical conductivity (Fig. 8e and f) that by supplying *a priori* knowledge about the peat depth, the distribution of layer conductivity values is reduced. Moreover, although not shown, the uncertainty in electrical conductivity for layers 1 and 2 is substantially reduced by supplying *a priori* knowledge. The uncertainty for the depths of layer 1 in the unconstrained inversion is further indicated in Fig. 8d. The standard deviation of modeled depths where the model had a total misfit of < 5% demonstrates that uncertainty exceeds 0.8 m, and highlights that a diverse range of models can be used to describe the data.

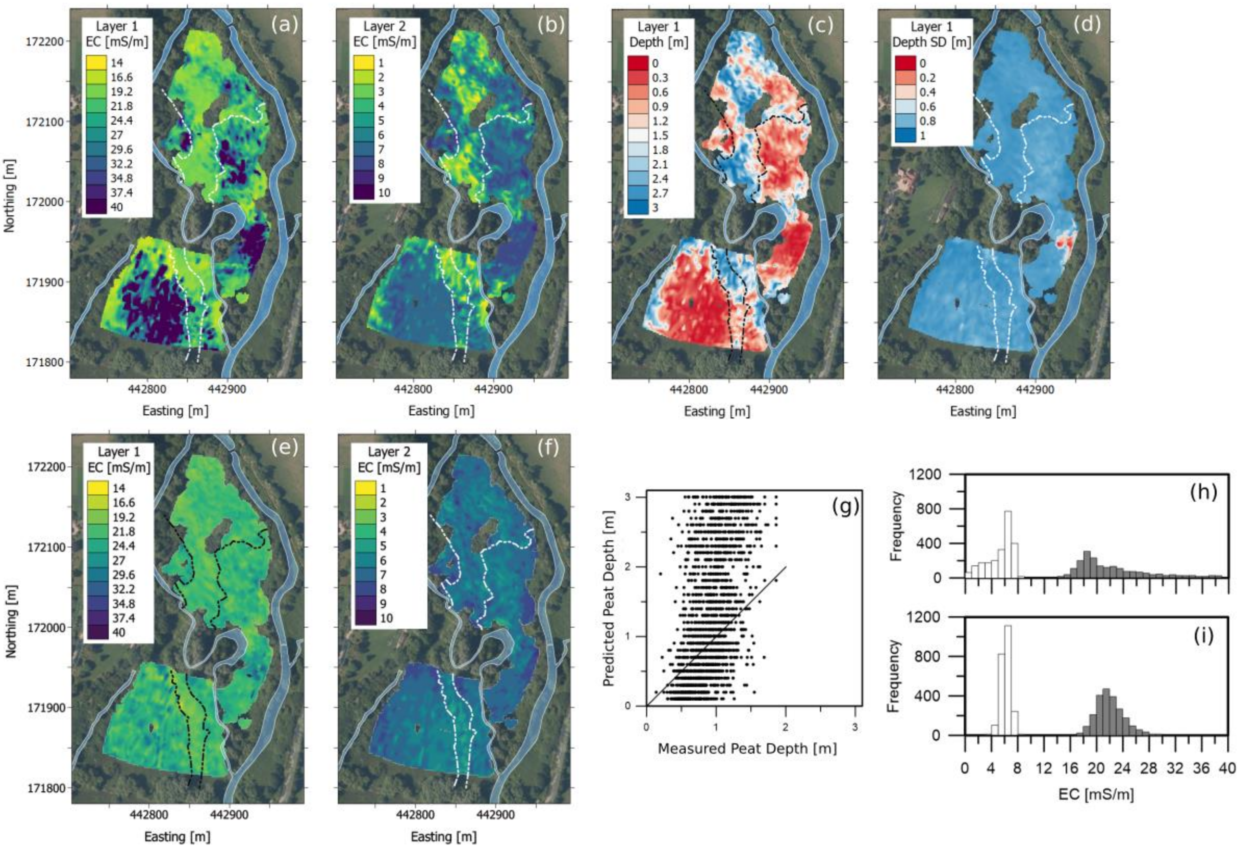

Figure 8 — Results of the sharp inversion approach for non-constrained and constrained cases: (a), (b), (c), and (d) show the layer 1 conductivities, layer 2 conductivities, layer 1 depths, and depth standard deviations of the unconstrained approach. (e) and (f) show the electrical conductivities of layers 1 and 2 in the constrained approach. (g) shows the pattern between the predicted and measured peat depths. (h) and (i) are histograms for the conductivities of layer 1 (grey) and layer 2 (white) for unconstrained and constrained cases. Dashed lines in map plots indicate the position of the peat channel.

3.3 Hydrogeological Characterization

Fig. 9 displays the correlations between *ECa* measurements, inversion results, and hydrogeological parameters. It was anticipated that there would be negative correlations between *ECa* and thickness of the saturated zone; however, none of the correlations were statistically significant (at the 5% level). Similarly, no significant relationships between *ECa* and peat hydraulic conductivity, gravel hydraulic conductivity, or gravel water electrical conductivity were observed.

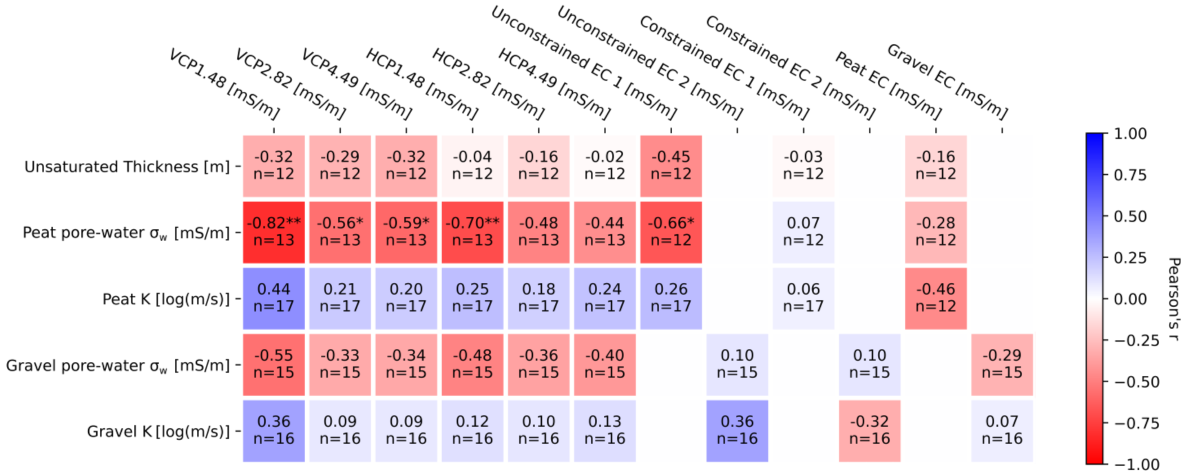

Figure 9 - Correlations between EMI measurements and hydrological parameters. *K* is used to represents permeability, σ_w represents pore-water conductivity. Significance levels are indicated as follows: * represents $p < 0.05$ and ** represents $p < 0.01$.

Curiously, however, it was observed that all VCP measurements and HCP1.48 measurements had a significant negative correlation with peat pore-water electrical conductivity. This could be explained if porosity was negatively correlated with peat pore-water electrical conductivity. For instance, areas with higher porosity may be flushed more readily by low conductivity rain waters. Such a hypothesis is somewhat backed by the correlation between peat water conductivity and log-transformed hydraulic conductivity of the peat (r = -0.67, p < 0.05, n = 12). However, it is important to note that the unconstrained layer 1 conductivity of the sharp inversion also displays a significant negative correlation. Given that such a correlation was not observed for the constrained sharp inversion, a negative correlation between pore-water electrical conductivity and peat depth is also expected. It is however important to note the strongest relationships for peat pore-water electrical conductivity are with VCP1.48 and HCP1.48, whereas for peat depths VCP4.49 and HCP2.82 had the strongest correlation, Fig 5.

The estimated porosities for the peats and gravels, following equations 2 and 3, resulted in average porosities of 0.424 (SD = 0.102) and 0.323 (SD = 0.004), respectively. The estimates for gravel are in agreement with gravels in similar environments (e.g. Frings et al., 2011). However, the porosities for the peats here are typically lower than in other environments (e.g. Walter et al., 2015). This can be attributed to an elevated proportion of silt and clay present in the peat deposits at the Boxford Wetland, see Newell et al. (2016). Additionally, the estimated peat porosity has a significant positive relationship with hydraulic conductivity (r = 0.60, p < 0.05), and provides additional validity to the hypothesis behind the observed correlation between pore-water conductivity and EMI values. Nonetheless, given that peat pore-water, electrical conductivity values are required to obtain porosities, a petrophysical relationship to predict the hydraulic conductivity across the site was not possible.

It is also worth noting that if the results from the smooth inversion are used to predict the porosities, the peats have an average porosity of 0.32 and the gravels have a porosity of 0.38. This is because the true electrical contrast between gravels and peats is reduced in the smooth inversion, and although the electrical conductivities for the gravels are lower than the peats their higher estimated porosities are a result of the absence of surface conductivity component in equation 2.

The synthetic modeling allows further investigation of the hydrogeological information content of the EMI data, the results are displayed in Fig. 10. As noted, the data were generated for a series of 4-layer models; layers 1 and 2 represent the unsaturated and saturated zones of the upper peat, layer 3 represents the lower peat and layer 4 represents the gravel. The correlation between changes in *ECa* and bulk electrical conductivities and changes in hydrological states are shown in Fig. 10. There is substantial potential to resolve changes in the upper peat and gravel pore-water conductivity from *ECa* values. However, for lower peat pore-water and unsaturated zone thickness the correlations are substantially weaker. Moreover, for the sharp inversion, it can be seen that although the layer conductivities of the unconstrained sharp inversion are high for the upper peat pore-water conductivity and moderate for the lower peat pore-water conductivity, the correlations are substantially improved for the constrained inversion.

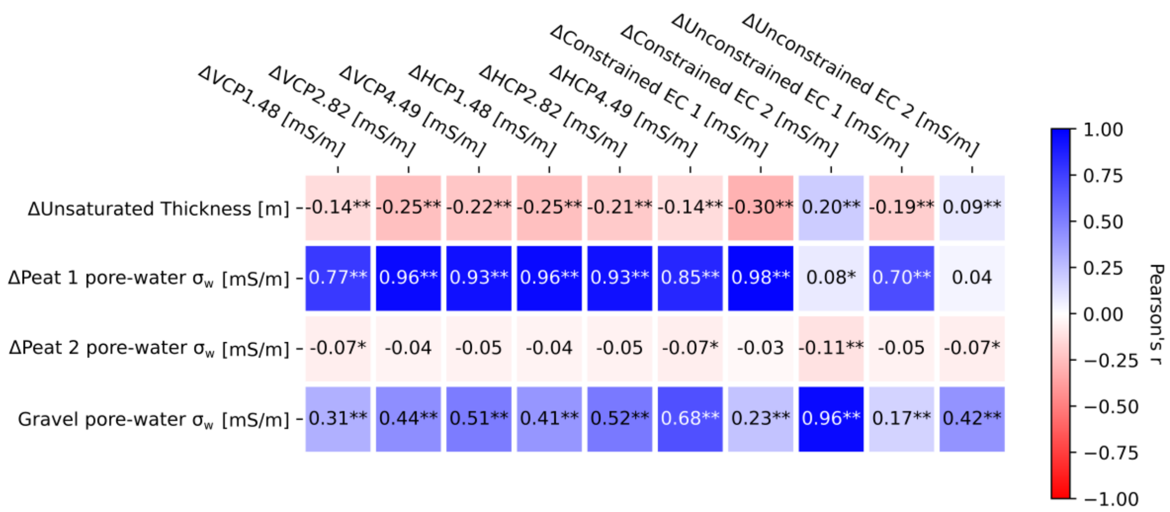

Figure 10 - Correlations between EMI measurements and hydrological parameters used in synthetic modeling. σ_w represents pore-water conductivity. Significance levels are indicated as follows: * represents $p < 0.05$ and ** represents $p < 0.01$.

It is important to also note here that, unlike Fig. 9, the correlations in Fig. 10 are expressed as changes, not as absolute values. Therefore, the poorer correlations between the measured pore-water conductivities with EMI data and inversion results can likely be attributed to additional variability in porosity, peat depth, and perhaps vegetation cover. Moreover, for the field data contrasts in spatial resolution of geophysical and hydrogeological parameters can cause additional factors to reduce the correlation, and although spatial averaging or interpolation methods may be able to improve correlation, it is an important issue to be cautious of. Nonetheless, it is evident that even if absolute values do not yield significant information about properties or states, this information may be present in appropriately collected time-lapse EMI data and enhanced resolution can be achieved with *a priori* knowledge. Moreover, it also follows that with the collection of more hydrogeological data more substantial relationships could be obtained.

4 Discussion

4.1 Acquisition and Calibration of EMI Data

In this work, EMI data were collected at an elevation of 1 m due to the vegetation at the site. This has several important implications. Firstly, as noted, the sensitivity patterns of the device are modified. Although the exact modifications of the sensitivity patterns will be dependent upon the subsurface conductivity, the approach investigated by Andrade and Fischer (2018) which uses McNeill's (1980) cumulative sensitivity function is validated by the observed similar values of the correlations between peat depths and VCP4.49 and HCP2.82 measurements, which have similar depth of investigation (4.6 and 4.5 m, respectively). Secondly, by elevating the device, the signal-to-noise ratio is reduced because the measurement magnitude is reduced, and the magnitude of errors is increased (e.g. device rotation or instability). Although some systematic errors are removed by ERT calibration, errors arising from variable acquisition errors or vegetation are still likely to influence the measurements. However, although some large errors were observed (see Fig. 2), most data had low errors.

Furthermore, although the factors mentioned above are likely to reduce the quality of data in similar environments, i.e. where vegetation precludes the use of all-terrain-vehicles and sleds, it is important to note that the walking survey here was still more productive than the 3D ERT investigation of Chambers et al. (2014). For instance, the EMI data collected here required 2-person-days to collect the data across the entire 10 ha field site, in comparison the work of Chambers et al. (2014) required 12-person-days. Furthermore, although the 3D ERT work provided superior characterization, the transport of numerous electrodes and cable spools may be unfeasible in remote sites, and if only shallow characterization is required, EMI offers a more attractive and rapid approach. ERT surveys are also more invasive (e.g., electrode placement and disturbance of vegetation), which can also be problematic in ecologically sensitive wetland environments.

In this work, data were calibrated using ERT models following the approach of Lavoué et al. (2011). Whilst it was observed that this substantially improved convergence of the EMI data, it should be noted that the depths of investigation of the ERT survey, as determined by the Oldenburg and Li (1999) method, were substantially smaller than the depth of investigation of the EMI device. Although they were calculated differently, the ERT calibration here was essentially biased to the shallower conductivity, in comparison to the deeper areas; this is the opposite of Rejiba et al. (2018) who hypothesized that their choice of ERT set up did not allow accurate calibration of the shallowest subsurface. Moreover, although lateral smoothing was used to reduce artifacts related to different spatial resolution, these effects were not investigated in significant detail. Other methods to calibrate data, e.g. electrical resistivity sounding (von Hebel et al., 2019), soil sampling (e.g. Moghadas et al., 2012), and multi-elevation EMI measurements (e.g. Tan et al., 2019) have been investigated and may offer superior methods to calibration. It is clear, however, that an objective study investigating these approaches and the depth of investigation of electrical resistivity methods (which is seldom reported) could go a long way in ascertaining the best approach in the calibration of EMI data.

4.2 Predicting Peat Depth using EMI methods

Although there is a range of EMI inversion software available, in this work EMagPy was used to produce smooth and sharp models of electrical conductivity. Ultimately, however, it was observed that of the approaches for determining peat depth, the multilinear regression method worked best. These findings agree with the recent work of Beucher et al. (2020) who found that the best approach for determining peat depth was using a linear regression method and that it performed better than inverse models obtained from Aarhus workbench. Moreover, given that at low conductivity values the ERT calibration is assumed linear, by-passing the ERT calibration of the EMI data does not substantially reduce the performance of the multi-linear regression prediction method. For instance, using uncalibrated EMI data and 100 peat depth observations yielded a relationship with an NMAD of 18.6%, in comparison to the NMAD of 18.3% when using calibrated data.

In this work, it is evident that the electrical conductivities of the unconstrained sharp inversion are highly correlated with the measured peat depths, i.e. high first layer electrical conductivities are correlated with small first layer thicknesses. This is a crucial limitation of this approach, and although it could be argued that regularization could be introduced this may reduce the accuracy of petrophysical interpretations. Potentially, the results of a non-regularized inversion could be improved by adding electrical conductivity bounds. For example, von Hebel (2014) proposed using bounds of double the maximum *ECa* value and half the minimum *ECa* value when the device was operated at ground level. Although this approach can be modified for cases where the device is elevated, such an approach would be too conservative to resolve the contrasting gravel and peat conductivities (as observed in the ERT results) at this field site. The failure of this method, i.e. high uncertainty in final models (see Fig. 8d), is likely a result of the underdetermined nature of the inverse problem, as although six measurements were obtained, they are noisy and are not truly independent. Furthermore, the similarity of measurements is increased by operating the device above the ground. For future applications retaining the lack of vertical regularization, the uncertainty of the problem could perhaps be reduced by using lateral smoothing, collecting more measurements with different sensitivity patterns, or operating the device at the ground.

Additionally, although the predictions using the smooth inversion were substantially better, they were not as good as the multi-linear regression method. This is likely due to a combination of regularisation and discretization of the model which acts to smooth the boundaries. For instance, one could argue that given that the inversions are conducted independently, it is not necessary to use the same vertical regularization and model discretization. Although this may improve peat depth prediction, one cannot arbitrarily pick vertical smoothing values to obtain the best correlation. Nonetheless, it is possible that using an objective approach, such as an L-curve, could help to select independent vertical smoothing values for each 1D inversion. This however invokes a substantial increase in computation time, especially if Full-Maxwell forward models are used.

4.3 Obtaining Hydrogeological Information

In addition to characterizing wetland structure, there is interest in obtaining both static and dynamic hydrogeological information about wetlands. Given the dependence of EMI measurements on peat depth the data ought to be governed by contrasts in the hydrogeological properties between the peats and gravels. For instance, given the similarities of pore-water conductivities at the time of sampling, the contrasts can most likely be linked to porosity. The negative correlation between VCP measurements, HCP1.48, the unconstrained layer 1 conductivity of the sharp inversion, and peat pore-water conductivity highlight the negative correlation between peat depth and porewater conductivity. However, the similarly strong negative correlation between peat pore-water conductivity and log-transformed conductivity highlight more intrusive information is required. For instance, by collecting a larger set of intrusive information, the influence of uncorrelated variability could be mitigated, and meaningful observations could be observed.

Using Archie's (1942) law for the gravel and a modified Archie's law (Comas and Slater, 2004) for the peats it was possible to obtain estimates of porosity. As noted, when the values from electrical conductivity from the smooth inversion were used, the estimates for porosity were significantly lower than those obtained when using electrical conductivity values from the sharp models. In the synthetic work, it was observed that there is substantial potential for time-lapse EMI to reveal dynamic patterns. Furthermore, although site-specific relationships could be developed to link *ECa* and hydrogeological parameters, inversion results (and therefore the use of established petrophysical relationships), were significantly better if structural information was supplied. Perhaps this information could be supplied by ground-penetrating radar surveys which have proved successful in the past (Slater and Comas et al., 2004; Walter et al., 2015).

5 Conclusions and Outlook

The potential of EMI methods to characterize the hydrogeological structure was assessed, using a combination of intrusive measurements and synthetic modeling. EMI data were calibrated using the ERT data and errors were quantified using cross-over points. Here, the depth of investigation of the ERT was relatively shallow in comparison to the EMI sensitivity; future applications ought to investigate the influence of differences in both vertical and spatial resolution between both methods (see also von Hebel et al., 2019).

Calibrated EMI data were inverted using both smooth and sharp inversion algorithms, however, the absence of regularization in the sharp inversion resulted in large degrees of uncertainty in the resulting models. Moreover, because of the extensive data set of intrusive measurements it was possible to objectively assess the performance of the sharp inversion algorithm. Consideration of this uncertainty is important and future applications could reduce it using intrusive information or collection of more EMI measurements with different sensitivity patterns.

Although the smooth inversions permitted characterization of the peat depth with relatively good accuracy, a method using the EMI data and a multi-linear regression model provided superior accuracy. Given the substantial contrasts in hydrogeological properties of the peats and gravels, this structural information is valuable for determining conceptual models of the field site. Such characterization could help to inform management decisions in similar environments and aid in the management and restoration of wetlands.

However, although it was possible to distinguish between peat and gravel, no meaningful petrophysical relationships linking hydrogeological properties with EMI data were obtained. This could be attributed to the variability of static properties (e.g. peat depth and porosity) and the influence of different vegetation cover across the field site, however, it is possible that with additional hydrogeological measurements more meaningful relationships could be obtained.

Moreover, although estimates of porosity were obtained from the sharp inversion methods, when using the electrical conductivities obtained from the smooth models, the predicted peat porosities were likely underestimated and whereas the gravel porosities were likely overestimated. This is an important consideration in stratified environments, because although electrical properties are likely to vary smoothly within lithologies, ideally regularization across boundaries should be limited to obtain the most accurate petrophysical interpretations.

Lastly, the synthetic component permitted removal of variability associated with the porosity and structural heterogeneity, and vegetation cover, to focus solely on change water content and pore-water electrical conductivity. In doing so the potential for EMI to characterize dynamic properties in the wetland was revealed. It is however important to note that as EMI measurements are prone to drift and influence of the user, it would be necessary to calibrate the device. Nonetheless, the application of time distributed EMI surveys has clear relevance for understanding groundwater-surface water dynamics at the site, which is important for both the local ecosystem and the wider climate (e.g. related CO_2 and CH_4 production).

lateral resolution can benefit from the provided information.

References

Allen, D.J., Darling, W.G., Gooddy, D.C. (2010). Interaction between groundwater, the hyporheic zone and a Chalk stream: a case study from the River Lambourn, UK. Hydrogeol J 18, 1125–1141. https://doi.org/10.1007/s10040-010-0592-2

Andrade, F., Fischer, T., Valenta, J. (2016). Study of Errors in Conductivity Meters Using the Low Induction Number Approximation and How to Overcome Them. 10.3997/2214-4609.201602080.

Andrade, F., Fischer, T. (2018). Generalised relative and cumulative response functions for electromagnetic induction conductivity meters operating at low induction numbers. Geophysical Prospecting. 66. 595-602. 10.1111/1365-2478.12553.

Archie, G.E. (1942). "The electrical resistivity log as an aid in determining some reservoir characteristics". Petroleum Transactions of AIME. 146: 54–62. doi:10.2118/942054-g.

Auken, E., Christiansen, A., Kirkegaard, C., Fiandaca, G., Schamper, C., Behroozmand, A., Binley, A., Nielsen, E., Efferso, F., Christensen, N., Sørensen, K., Foged, N., Vignoli, G. (2014). An overview of a highly versatile forward and stable inverse algorithm for airborne, ground-based and borehole electromagnetic and electric data. Exploration Geophysics. 10.1071/EG13097.

Beucher, A., Koganti, T., Iversen, B., Greve, M. (2020). Mapping of Peat Thickness Using a Multi-Receiver Electromagnetic Induction Instrument. Remote Sensing. 12. 21. 10.3390/rs12152458.

Binley, A., Hubbard, S. S., Huisman, J. A., Revil, A., Robinson, D. A., Singha, K., and Slater, L. D. (2015), The emergence of hydrogeophysics for improved understanding of subsurface processes over multiple scales, Water Resour. Res., 51, 3837– 3866, doi:10.1002/2015WR017016.

Blanchy, G., Saneiyan, S., Boyd, J., McLachlan, P., Binley, A. (2020) ResIPy, an intuitive open source software for complex geoelectrical inversion/modeling, Computers & Geosciences, Volume 137, 104423, ISSN 0098-3004, https://doi.org/10.1016/j.cageo.2020.104423.

Brosten, T., Day-Lewis, F., Schultz, G., Curtis, G., Lane, J. (2011). Inversion of multi-frequency electromagnetic induction data for 3D characterization of hydraulic conductivity. Journal of Applied Geophysics. 73. 323-335. 10.1016/j.jappgeo.2011.02.004.

Callegary, J., Ferré, T., Groom, R. (2007). Vertical Spatial Sensitivity and Exploration Depth of Low-Induction-Number Electromagnetic-Induction Instruments. Vadose Zone Journal. 6. 158-167. 10.2136/vzj2006.0120.

Chambers, J., Wilkinson, P., Uhlemann, S., Sorensen, J., Roberts, C., Newell, A., Ward, W., Binley, A., Williams, P., Gooddy, D. (2014) Derivation of lowland riparian wetland deposit architecture using geophysical image analysis and interface detection. Water Resour Res 50:5886–5905

Comas, X., Slater, L., and Reeve, A. (2005), Geophysical and hydrological evaluation of two bog complexes in a northern peatland: Implications for the distribution of biogenic gases at the basin scale, Global Biogeochem. Cycles, 19, GB4023, doi:10.1029/2005GB002582.

Comas, Xavier & Slater, Lee. (2004). Low-frequency electrical properties of peat. Water Resources Research - Water Resour Res. 401. 10.1029/2004WR003534.

Corwin, D. (2008). Past, present, and future trends of soil electrical conductivity measurement using geophysical methods. Handbook of Agricultural Geophysics.

Dafflon, B., Hubbard, S., Ulrich, C., Peterson, J.E. (2013), Electrical Conductivity Imaging of Active Layer and Permafrost in an Arctic Ecosystem, through Advanced Inversion of Electromagnetic Induction Data. Vadose Zone Journal, 12: 1-19 vzj2012.0161. doi:10.2136/vzj2012.0161

Davidson, N. (2014). How much wetland has the world lost? Long-term and recent trends in global wetland area. Marine and Freshwater Research. 65. 936-941. 10.1071/MF14173.

Frederiksen, R.,Christiansen, A., Christensen, S., Rasmussen, K. (2017). A direct comparison of EMI data and borehole data on a 1000 ha data set. Geoderma. 303. 188-195. 10.1016/j.geoderma.2017.04.028.

Grapes, T., Bradley, C., Petts, G. (2006). Hydrodynamics of floodplain wetlands in a chalk catchment: the River Lambourn, UK. Journal of Hydrology. 320 (3-4), pp. 324-341. https://doi.org/10.1016/j.jhydrol.2005.07.028

Heiri, O., Lotter, A., Lemcke, G. (2001) Loss on ignition as a method for estimating organic and carbonate content in sediments: reproducibility and comparability of results. Journal of Paleolimnology 25, 101–110 (2001). https://doi.org/10.1023/A:1008119611481

Holden, J., Burt, T., Vilas, M.. (2002). Application of ground-penetrating radar to the identification of subsurface piping in blanket peat. Earth Surface Processes and Landforms. 27. 10.1002/esp.316.

House, A. R., Thompson, J. R., Sorensen, J. P. R., Roberts, C., and Acreman, M. C. (2016) Modelling groundwater/surface water interaction in a managed riparian chalk valley wetland. Hydrol. Process., 30: 447– 462. doi: 10.1002/hyp.10625.

House, A.R., Thompson, J.R., Acreman, M.C. (2016). Projecting impacts of climate change on hydrological conditions and biotic responses in a chalk valley riparian wetland, Journal of Hydrology, Volume 534

House, A., Sorensen, J., Gooddy, D., Newell, A., Marchant, B., Mountford, J. Scarlett, P., Williams, P., Old, G. (2015). Discrete wetland groundwater discharges revealed with a three-dimensional temperature model and botanical indicators (Boxford, UK). Hydrogeology Journal. 23. 10.1007/s10040-015-1242-5.

Lavoué, F., Kruk, J., Rings, J. Andre, F., Moghadas, D., Huisman, J., Lambot, S. Weihermüller, L., Vanderborght, J., Vereecken, H. (2010). Electromagnetic induction calibration using apparent electrical conductivity modelling based on electrical resistivity tomography. Near surface geophysics. 8. 553-561. 10.3997/1873-0604.2010037.

McLachlan, P., Blanchy, G., Binley, A., EMagPy: Open-source standalone software for processing, forward modeling and inversion of electromagnetic induction data, Computers & Geosciences, Volume 146, 2021,

McLachlan, P., Chambers, J., Uhlemann, S., Sorensen, J. and Binley, A. (2020), Electrical resistivity monitoring of river–groundwater interactions in a Chalk river and neighbouring riparian zone. Near Surface Geophysics, 18: 385-398. doi:10.1002/nsg.12114

McLachlan, P.J., Chambers, J.E., Uhlemann, S.S., et al. (2017) Geophysical Characterization of the Groundwater Surface Water Interface. Advances in Water Resources, 109, 302-319.

Mitsch, W., Bernal, B., Nahlik, A., Mander, Ü., Zhang, L., Anderson, C., ,Jørgensen, S., Brix, H. (2012). Wetlands, carbon, and climate change. Landscape Ecology. 28. 10.1007/s10980-012-9758-8.

Monteiro-Santos, F. A., (2004). 1-D laterally constrained inversion of EM34 profiling data. Journal of Applied Geophysics, 56(2), 123-134, doi:http://dx.doi.org/10.1016/j.jappgeo.2004.04.005.

Newell, A., Sorensen, J., Chambers, J., Wilkinson, P., Uhlemann, S., Roberts, C., Gooddy, D., Vane, C., Binley, A.. (2015). Fluvial response to Late Pleistocene and Holocene environmental change in a Thames chalkland headwater: The Lambourn of southern England. Proceedings of the Geologists' Association. 126. 10.1016/j.pgeola.2015.08.008.

Newell, A., Vane, C., Sorensen, J., Moss-Hayes, V., Gooddy, D. (2016). Long-term Holocene groundwater fluctuations in a chalk catchment: evidence from Rock-Eval pyrolysis of riparian peats: Rock-Eval evidence for groundwater fluctuations in a chalk catchment. Hydrological Processes. 30. 10.1002/hyp.10903.

Old, G.H., Naden, P.S., Rameshwaran, P., Acreman, M.C., Baker, S., Edwards, F.K., Sorensen, J.P.R., 624 Mountford, O., Gooddy, D.C., Stratford, C.J., Scarlett, P.M., Newman, J.R., Neal, M., (2014). Instream 625 and riparian implications of weed cutting in a chalk river. Ecological Engineering 71, 290-300

Oldenburg, D., Li. (1999) Estimating depth of investigation in dc resistivity and IP surveys GEOPHYSICS, 64(2):403

Parsekian, A. D., Singha, K., Minsley, B. J., Holbrook, W. S.,, Slater, L. (2015), Multiscale geophysical imaging of the critical zone. Rev. Geophys., 53, 1– 26. doi: 10.1002/2014RG000465.

Sherlock, M.D., McDonnell, J.J. (2003), A new tool for hillslope hydrologists: spatially distributed groundwater level and soilwater content measured using electromagnetic induction. Hydrol. Process., 17: 1965-1977. doi:10.1002/hyp.1221

Singha, K., Day-Lewis, F. D., Johnson, T., Slater, L. D. (2015), Advances in interpretation of subsurface processes with time-lapse electrical imaging, Hydrol. Process., 29; pages 1549– 1576, doi: 10.1002/hyp.10280

Uhlemann, S.S., Sorensen, J. P. R., House, A. R., Wilkinson, P. B., Roberts, C., Gooddy, D. C., Binley, A. M., Chambers, J. E. (2016), Integrated time-lapse geoelectrical imaging of wetland hydrological processes, Water Resour. Res., 52, 1607– 1625, doi:10.1002/2015WR017932.

von Hebel, C., Rudolph, S., Mester, A., Huisman, J. A., Kumbhar, P., Vereecken, H., van der Kruk, J. (2014), Three-dimensional imaging of subsurface structural patterns using quantitative large-scale multiconfiguration electromagnetic induction data, Water Resour. Res., 50, 2732– 2748, doi:10.1002/2013WR014864.

von Hebel, C.; van der Kruk, J.; Huisman, J.A.; Mester, A.; Altdorff, D.; Endres, A.L.; Zimmermann, E.; Garré, S.; Vereecken, H. (2019). Calibration, Conversion, and Quantitative Multi-Layer Inversion of Multi-Coil Rigid-Boom Electromagnetic Induction Data. Sensors, 19, 4753.

Wagner, K., Gallagher, S., Hayes, M., Lawrence, B., Zedler, J. (2008). Wetland Restoration in the New Millennium: Do Research Efforts Match Opportunities?. Restoration Ecology. 16. 367 - 372. 10.1111/j.1526-100X.2008.00433.x.

Walter, J., Lück, E., Bauriegel, A., Richter, C. and Zeitz, J. (2015), Multi-scale analysis of electrical conductivity of peatlands for the assessment of peat properties. Eur J Soil Sci, 66: 639-650. doi:10.1111/ejss.12251

Whalley, W., Binley, A., Watts, C. (2017) Methods to estimate changes in soil water for phenotyping root activity in the field. Plant Soil 415, 407–422 https://doi.org/10.1007/s11104-016-3161-1

Younger,P. L. (1989) Devensian periglacial influences on the development of spatially variable permeability in the Chalk of southeast England Quarterly Journal of Engineering Geology and Hydrogeology, 22(4):343